The Prospect for Remote Sensing of Cirrus Clouds with a Submillimeter-Wave Spectrometer

K. FRANKLIN EVANS AND AARON H. EVANS

Program in Atmospheric and Oceanic Sciences, University of Colorado, Boulder, Colorado

IRA G. NOLT

NASA/Langley Research Center, Hampton, Virginia

B. THOMAS MARSHALL

GATS, Inc., Hampton, Virginia

(Manuscript received 1 December 1997, in final form 22 July 1998)

ABSTRACT

Given the substantial radiative effects of cirrus clouds and the need to validate cirrus cloud mass in climate models, it is important to measure the global distribution of cirrus properties with satellite remote sensing. Existing cirrus remote sensing techniques, such as solar reflectance methods, measure cirrus ice water path (IWP) rather indirectly and with limited accuracy. Submillimeter-wave radiometry is an independent method of cirrus remote sensing based on ice particles scattering the upwelling radiance emitted by the lower atmosphere.

A new aircraft instrument, the Far Infrared Sensor for Cirrus (FIRSC), is described. The FIRSC employs a Fourier Transform Spectrometer (FTS), which measures the upwelling radiance across the whole submillimeter region (0.1–1.0-mm wavelength). This wide spectral coverage gives high sensitivity to most cirrus particle sizes and allows accurate determination of the characteristic particle size.

Radiative transfer modeling is performed to analyze the capabilities of the submillimeter FTS technique. A linear inversion analysis is done to show that cirrus IWP, particle size, and upper-tropospheric temperature and water vapor may be accurately measured. A nonlinear statistical algorithm is developed using a database of 20 000 spectra simulated by randomly varying most relevant cirrus and atmospheric parameters. An empirical orthogonal function analysis reduces the 500-point spectrum (20–70 cm^{-1}) to 15 ''pseudo-channels'' that are then input to a neural network to retrieve cirrus IWP and median particle diameter. A Monte Carlo accuracy study is performed with simulated spectra having realistic noise. The retrieval errors are low for IWP (rms less than a factor of 1.5) and for particle sizes (rms less than 30%) for IWP greater than 5 g m^{-2} and a wide range of median particle sizes. This detailed modeling indicates that there is good potential to accurately measure cirrus properties with a submillimeter FTS.

1. Introduction

The importance of cirrus clouds to the earth's radiation budget is widely understood. Cirrus is pervasive, covering at least 20% of the earth (Wylie et al. 1994). Due to their cold temperatures, cirrus clouds may have a net warming effect (from longwave trapping) or a net cooling effect (from shortwave reflection), depending on their optical properties (Stephens and Webster 1981; Liou 1986). Our ability to model the radiative effects of cirrus is poor due to uncertainties in predicting cloud formation, vertical and horizontal extent, and microphysical properties such as ice water path (IWP) and ice particle size. There are also substantial difficulties in modeling the optical properties and radiative effects from the microphysical properties and geometric structure of cirrus clouds (Stephens et al. 1990). To improve their representation of cirrus clouds, climate models now have cloud parameterizations that predict cloud ice mass (e.g., Fowler et al. 1996). The conservation of water mass principle provides a physical basis to predict the various components of the hydrologic cycle. Thus it is important to make global observations of cirrus cloud mass (IWP) and particle size in addition to optical depth and radiative fluxes. Satellite remote sensing, especially passive sensors, offers the most practical method for long-term global monitoring of these cloud properties (Wielicki et al. 1995).

Corresponding author address: K. Franklin Evans, Program in Atmospheric and Oceanic Sciences, University of Colorado, Campus Box 311, Boulder, CO 80309.
E-mail: evans@nit.colorado.edu

No single remote sensing technique will be able to provide accurate measurements of cirrus IWP and optical depth for the full range of cloud situations. Solar reflectance techniques for cirrus (e.g., Wielicki et al. 1990) convert reflectance to optical depth using phase functions that are highly sensitive to particle shape (Minnis et al. 1993). Surface reflectance and aerosol uncertainties become important for optically thin cirrus. There are substantial errors from vertical and horizontal inhomogeneities in clouds that are not optically thin. Additional errors are introduced when optical depth is converted to ice water path with effective particle sizes inferred with an absorbing reflectance channel. Thermal infrared methods require knowledge of the clear sky and cloud temperature (Inoue 1985; Giraud et al. 1997) or parameterizations relating temperature and particle size (Ou et al. 1993). Infrared techniques become insensitive for particle diameters larger than about 100 μm or absorption optical depths greater than two. All remote sensing methods from radar to visible have substantial inaccuracy due to uncertainties in cirrus ice particle shape.

Given the uncertainties associated with existing cirrus remote sensing techniques, it is valuable to pursue new remote sensing methods that are based on substantially different physics. One reason is the difficulty in validating satellite algorithms with in situ and ground-based methods. The small in situ and active sensor volumes and limited number of cases coincident with satellite pixels result in large sampling errors. New independent remote sensing methods will lead to improved understanding of the strengths and weaknesses of all the techniques, and ultimately lead to a combined sensor approach as the optimum method. Here we focus on a new far infrared/submillimeter technique for sensing cirrus properties.

The utility of the submillimeter part of the spectrum for passive sensing of cirrus was first discussed in Gasiewski (1992) and further explored in Evans and Stephens (1995). More recently, detailed modeling of the technique was performed in Evans et al. (1998). At submillimeter frequencies (>300 GHz) the lower atmosphere emits relatively uniformly, while the surface contribution to upwelling radiation is effectively blocked due to water vapor absorption. Cirrus ice particles scatter some of this upwelling radiation back down. To an observer above a cirrus cloud, the scattering decreases the brightness temperature from the clear-sky value. As the wavelength of microwave radiation decreases toward the sizes typical of cirrus particles, the sensitivity to cirrus ice mass increases dramatically. The change in brightness temperature depends on the cirrus IWP, particle size, and shape. Evans et al. (1998) developed a simple two-channel technique that was capable of retrieving IWP and particle size. Frequencies in the transmission windows near 650 and 850 GHz were shown to be the most sensitive to cirrus for frequencies below 1000 GHz. An additional channel on the 183-GHz water vapor line was suggested for determining the ''background'' brightness temperature for no cirrus conditions.

Submillimeter remote sensing has a number of advantages that complement visible and infrared techniques. Since the wavelength of submillimeter radiation is comparable to the size of ice particles in cirrus clouds, observed brightness temperature changes from cirrus are well correlated to ice mass. This contrasts with visible and infrared methods, which operate in the geometric optics limit where the signal is proportional to the particle area. Microwave radiation interacts with ice particles primarily through scattering so that cloud emission and temperature are relatively unimportant. The radiative transfer tends to occur in a linear regime, which means that the signal is proportional to the average cirrus properties in the field of view, and the effects of cloud inhomogeneity are minimized. Evans et al. (1998) performed error analyses, including the effects of particle shape, size distribution, and cloud height, and found promising retrieval accuracy for cirrus IWP and particle size.

In addition to the microwave heterodyne approach to submillimeter radiometry, Fourier transform spectrometry (FTS) provides a means to measure atmospheric radiance. The wide FTS spectral range is useful for obtaining information about a range of particle sizes, while the high spectral resolution may allow correction for the effects of the water vapor profile. Furthermore, since the spectral resolution in FTS is determined by the maximum optical path difference, it is possible to adjust the observing parameters for an optimum trade-off between spectral resolution and spectrum scan time. On the other hand, the FTS scan (integration) time is much longer than for a heterodyne receiver, so fewer measurements may be obtained. Thus, there is basically a spectral bandwidth advantage for FTS versus a better spatial coverage advantage for the heterodyne. Finally, a far infrared FTS requires a broadband, cryogenically cooled bolometer detector.

In this paper we explore the submillimeter (mainly 20–70 cm^{-1}) FTS technique for remote sensing of cirrus. A new FTS instrument for cirrus sensing is described in section 2. The cirrus remote sensing potential of this instrument is evaluated by modeling spectral radiative transfer including molecular absorption (with a line-by-line model) and scattering (mainly with Mie theory). Forward modeling and a linear inversion analysis is done to determine the information contained in the submillimeter spectra (section 4). A neural network algorithm for retrieval of cirrus IWP and particle size is developed and tested (section 5).

2. The far infrared sensor for cirrus (FIRSC) instrument

Previous studies (Evans et al. 1998) of a two-channel microwave instrument for measuring cirrus properties provided the initial basis for designing a complementary

broadband spectral measurement based on Fourier transform spectrometry. The primary goal of this instrument design is to measure the upwelling submillimeter radiance in the spectral region from 10 to 70 cm^{-1}, which is relatively transparent in the upper troposphere. In past years a considerable effort has been invested in submillimeter FTS instrumentation for stratospheric trace gas analysis from aircraft (Nolt and Stearns 1980) and balloon platforms (Nolt et al. 1997; Carli et al. 1984). From this basis of experience a prototype FTS aircraft instrument for cirrus has been designed and built in a joint university and international collaboration.

An existing aircraft FTS system was upgraded with new mirror drive and detector systems at the University of Oregon. The original Michelson flat mirrors were replaced by dihedral mirrors to operate as a polarization-sensitive Martin–Puplett interferometer (Martin and Puplett 1969). In a Martin–Puplett interferometer configuration, the beamsplitter is a linearly polarizing grid that serves to divide the incident radiation into two orthogonally polarized components, one reflected to a fixed mirror arm and other transmitted to the scanning mirror. The fixed and moving mirrors are dihedral mirrors (i.e., rooftop), which act to rotate the plane of polarization by 90° upon reflection. Thus, the initially transmitted beam is reflected upon its return to the beamsplitter, and vice versa for the other arm. The recombined output beam is directed to an output polarizer that has its axis rotated 45° relative to the beamsplitter grid and directs the transmitted/reflected components to two separate detectors. The two detector outputs can have the same or, as in our case, different spectral passbands. The difference in the orthogonal polarized intensity components [which can be aligned to the vertical (V) and horizontal (H) planes] of the input source produces the interferometric modulation in the detected signal. The Fourier transform provides the spectrum of the V and H difference in intensity. For viewing nadir radiance, which is assumed to be unpolarized, an additional polarizer is placed in the input beam (its axis rotated 45° relative to the beamsplitter), which serves to reflect one plane of radiation from the nadir beam and transmit the orthogonal plane from a blackbody reference. The spectrum in this case is the brightness temperature difference between the nadir source and blackbody reference.

The cryogenic two-channel detector system was designed at Queen Mary and Westfield College based upon a similar system developed for the European SAFIRE-Airborne program (Dickinson et al. 1995). The Far Infrared Sensor for Cirrus (FIRSC) instrument uses two spectral channels to span the range between 10 and 135 cm^{-1}; the lower range from 10 to 70 cm^{-1} (half–power point) being sensed with a bolometer cooled to 0.3 K, and the 80 to 135 cm^{-1} range with an unstressed Ge:Ga photodetector cooled to 4.2 K.

For its initial flight tests, the FTS was installed in NASA's T-39 (Sabreliner) aircraft and viewed the radiance through a nadir-mounted polyethylene window. Cold optics and filtering inside the cryostat define the spectral bandpass and field of view, which is nearly independent of wavenumber. For inflight calibration, the nadir sky source is repaced by an ambient temperature blackbody providing a spectrum for a known source—reference temperature difference. This provides the needed reference spectrum to normalize the sky spectral intensity to units of equivalent brightness temperature. Figure 1 is a drawing of the FIRSC instrument.

Table 1 compares the observing parameters for FIRSC to the University of Wisconsin's High Resolution Interferometer Sounder (HIS). HIS operates routinely on the ER-2 and could provide complementary midinfrared radiance data. The intent is to match the scan parameters of the FIRSC instrument to those of HIS to enable synergistic combination of data from both instruments in future field validation programs. Together HIS and FIRSC would span the full nonopaque infrared spectral range.

The only detectors available for a far infrared FTS are bolometers, and, therefore, the signal-to-noise ratio at the longer wavelengths decreases proportionately to the scene radiance. In the Rayleigh–Jeans limits the intensity (power) per unit frequency is proportional to frequency squared. Based on calibration scans, we estimate the rms noise to be 1 K at 30 cm^{-1}, and scaling approximately according to $1/\nu^2$ with wavenumber ν. However, for defining the broad-scale cirrus signatures, the detector noise (precision) will be improved by the effective averaging of the high spectral resolution data in the retrieval process.

The FIRSC operated successfully during its first flight deployment in April and May 1998.

3. Modeling methods

a. Radiative transfer methods

Spectra are modeled based upon the projected FIRSC performance in order to understand the information content for cirrus and to develop a retrieval algorithm. In expectation of the aircraft flight ceiling the modeling is done for a nadir-viewing configuration from 12 km in winter U.S. continental atmospheres. The spectra modeled are at a resolution of 0.1 cm^{-1} from 20 to 70 cm^{-1}. This spectral range was chosen based on adequate instrument signal-to-noise ratio ($<$20 cm^{-1} has very high noise), clearer atmospheric transmission windows, and lower water vapor continuum uncertainties (as compared to above 70 cm^{-1}).

The molecular absorption by H_2O, O_2, and O_3 in this spectral region is computed with LINEPAK (Gordley et al. 1994), a line-by-line model. The Clough water vapor continuum (CKD_2.1) (Clough 1994) is included. The absorption profiles are computed at 0.01 cm^{-1} resolution and stored for later use in the radiative transfer. The radiative transfer is calculated at 0.01 cm^{-1} resolution and averaged over a triangular bandpass with

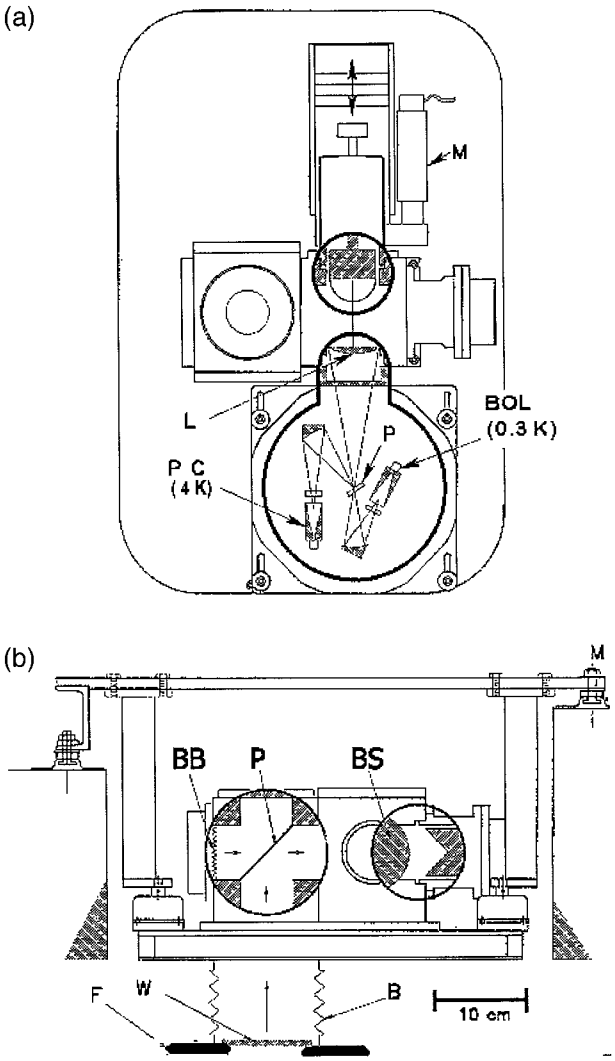

FIG. 1. Two views of the FIRSC instrument. (a) Cross sections of the motor-driven (M) dihedral mirror and the output lens (L), which images at a polarizer (P) in the 4.2 K optics of the cryostat. After this optical stop, reimaging cold optics and bandpass filters define the signal to the two detectors, a Ge:Ga photoconductor (PC) and a bolometer (BOL). (b) View looking forward at the FIRSC output where it enters the vacuum window to the cold optics and detector cryostat (not shown). The instrument is attached to the airplane floor (M) and views the upwelling radiance through a polethylene window (W) installed in the fuselage (F) and connected by a bellows (B) to maintain a dry instrument interior using a flow of dry gas He and N boiloff from the cryostat. The input polarizer (P) combines one linear polarization component of the sky with an orthogonal component of the blackbody (BB) as input to the beamsplitter (BS), which is a free-standing wire grid polarizer (with orientation rotated 45° relative to the input and output polarizers).

a full width at half maximum of 0.1 cm^{-1}. The absorption and radiative transfer are computed at a vertical resolution of 1–20 km maximum height, except at 0.25 km from 7 to 11 km (the cirrus region).

The absorption and scattering by cirrus clouds is calculated with a hybrid radiative transfer method that combines Eddington's second approximation with a single-scattering method (Deeter and Evans 1998). Since this radiative transfer algorithm is much faster than the line-by-line model, the molecular absorption is computed as a separate step. The cirrus ice particle distributions are represented by gamma distributions of an equivalent mass sphere diameter, D_e. The parameters of the gamma size distributions are the median diameter $D_{\rm me}$ and the width parameter α,

$$N(D) = aD_e^{\alpha} \exp[-(\alpha + 3.67)D_e/D_{\rm me}]. \quad (1)$$

The term D_e depends on the diameter D and particle shape and density; for solid spheres $D_e = D$. The relation between $D_{\rm me}$ and other measures of particle size depends on shape and α, but for solid spheres with $\alpha = 1$, $D_{\rm me} = 2.3r_e$, where r_e is the effective radius. The scattering information for randomly oriented ice particles is stored in a table at 0.5 cm^{-1} wavenumber resolution and 0.5 dB (factor of 1.122) $D_{\rm me}$ resolution. The scattering properties are delta-Eddington scaled.

Most of the modeling is done for solid spherical ice particles using Mie theory to make the scattering table. The index of refraction of ice is obtained from Warren (1984). Solid spheres may be a reasonable modeling choice for cirrus particles less than 100 μm (Heymsfield and McFarquhar 1996) but are suspect for larger ice particles. The use of equivalent mass distribution reduces the error, however. The effect of particle shape is briefly examined in the error analysis section where the scattering properties of ice cylinders are computed using the T-matrix code of Mishchenko (e.g., Mishchenko et al. 1996). A multistream doubling–adding radiative transfer code (Evans and Stephens 1991) is used to evaluate the fast hybrid transfer method for spectra computed from 20 to 70 cm^{-1}. For a homogeneous cloud with IWP = 10 g m^{-2} and $D_{\rm me}$ = 100 μm in a midlatitude winter atmosphere, the rms hybrid model nadir brightness temperature error is 0.27 K and the maximum error over the spectrum is 0.7 K. The rms error increases with IWP to 1.4 K at IWP = 100 g m^{-2}.

b. Cirrus case generation

To develop the algorithm a database is made containing many cirrus cloud cases embedded in a variety of atmospheres. The following cirrus parameters are randomly varied: IWP, median mass particle size ($D_{\rm me}$), gamma distribution width (α), cloud-top height ($Z_{\rm top}$), cloud-layer thickness (ΔZ), and IWC and $D_{\rm me}$ profile slopes (linear profiles assumed) within the cloud layer. The IWP and $D_{\rm me}$ are distributed according to a bivariate lognormal distribution with parameters obtained from 2D-C probe data from FIRE II. The IWP log mean corresponds to 9.6 g m^{-2}, standard deviation of the log is 1.68, and the maximum range is 2 to 200 g m^{-2}. The $D_{\rm me}$ log mean is 105 μm, standard deviation of the log is 0.63, and the maximum range is 30–300 μm. The correlation between ln(IWP) and ln($D_{\rm me}$) is 0.45. The term α takes on values of 0, 1, 2, and 7. The cloud is

TABLE 1. Measurement and instrument parameters for FIRSC and HIS.

Parameter	FIRSC	HIS
Bands (cm^{-1})	Band 1: 10–70 Band 2: 80–135	410–590, 590–1080 1080–1850, 2000–2700
Maximum resolution (cm^{-1})	0.1	0.8 to 1.8
Field of view (rad)	0.03	0.1
Footprint (km)	<1	<2
Input aperture (cm diam)	5.4	4.1
Scan time (s)	4	6
Maximum optical path difference (cm)	±5	±0.8 to 1.8
Mirror scan velocity (cm s^{-1})	1.25	0.6
Detectors	Band 1: bolometer @ 0.3 K Band 2: Ge:Ga @ 4 K	Si:Ar @ 6 K
Single scan SNR (ΔT_b rms)	About 1 K at 30 cm^{-1} decreasing as $1/\nu^2$	

constrained between 7 and 11 km. The top height varies uniformly, while the thickness is exponentially distributed with mean of 1.0 km. The microphysical profile slopes are uniformly distributed. The particles are assumed to be solid ice spheres. There is only a single vertically inhomogeneous cirrus layer and no liquid clouds.

The atmospheric temperature and water vapor profiles for the database are obtained from radiosonde data archived by the Atmospheric Radiation Measurement (ARM) program. In order to have a variety of atmospheric situations, 200 radiosonde profiles from December 1996 and January 1997 at the ARM Southern Great Plains site central facility are used. Because these soundings are not selected for having cirrus clouds, their water vapor content is probably biased low. The U.S. standard atmosphere profile of ozone is assumed (ozone is of minor importance). For each atmospheric profile 100 random cirrus clouds are generated. The radiative transfer procedure then calculates spectra for each cloud/atmosphere case giving a total of 20 000 spectra in the database.

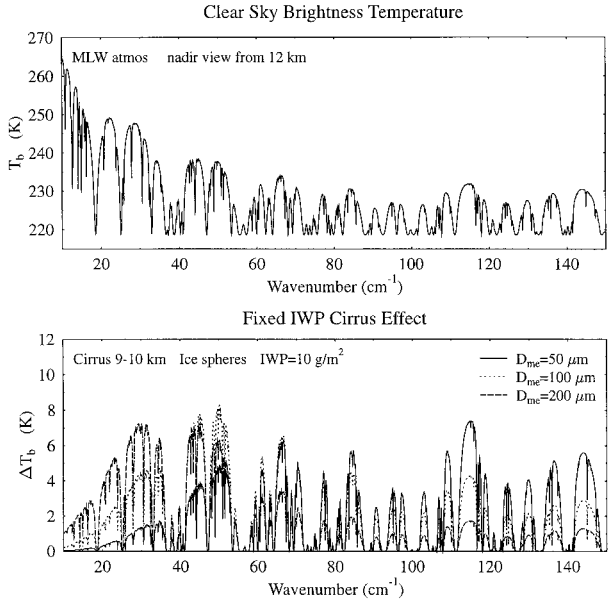

FIG. 2. (a) The far infrared brightness temperature spectrum computed for nadir viewing from 12 km in a standard midlatitude winter atmosphere. (b) The brightness temperature decrease due to a cirrus cloud with ice water path of 10 g m^{-2} and three different median ice sphere diameters, D_{me}.

4. The theoretical basis for submillimeter FTS sensing of cirrus

a. Forward radiative modeling

As an illustration of the radiance spectra the FIRSC instrument should obtain, the brightness temperature T_b modeled for an aircraft flying at 12 km in a midlatitude winter atmosphere is shown in Fig. 2. The higher T_b below 50 cm^{-1} indicate that the atmosphere is more transmissive in the lower wavenumber windows than the higher wavenumber ones. Assuming the water vapor continuum is somewhat correct, the windows above 70 cm^{-1} can still sense part of the upper troposphere. Figure 2 also shows the effect of modeled cirrus clouds on the radiance spectra. For fixed ice water path the lower wavenumbers are most sensitive to larger ice particles (e.g., $D_{me} = 200$ μm), while the higher wavenumbers are more sensitive to the smaller particles (e.g., $D_{me} = 50$ μm). The relative sensitivity to these ranges of particle sizes is fairly constant above 100 cm^{-1}.

A comparison of the submillimeter and mid-IR sensitivity to cirrus is shown in Fig. 3. The submillimeter and mid-IR sensitivity (ΔT_b) to cirrus is comparable, although the radiative processes are much different. It is clear from comparing the fixed IWP and fixed visible optical depth mid-IR spectra that the infrared brightness temperature change is sensing the optical depth and not the ice mass. The mid IR has only a slight sensitivity (around 12 μm) to this range of particle sizes. In contrast the submillimeter has considerable sensitivity to particle size for fixed IWP, as shown by how the relative ΔT_b for the different particle sizes varies across the spectrum. For wavenumbers less than 25 cm^{-1} the ΔT_b is much greater for $D_{me} = 200$ μm than for $D_{me} = 50$ μm, while

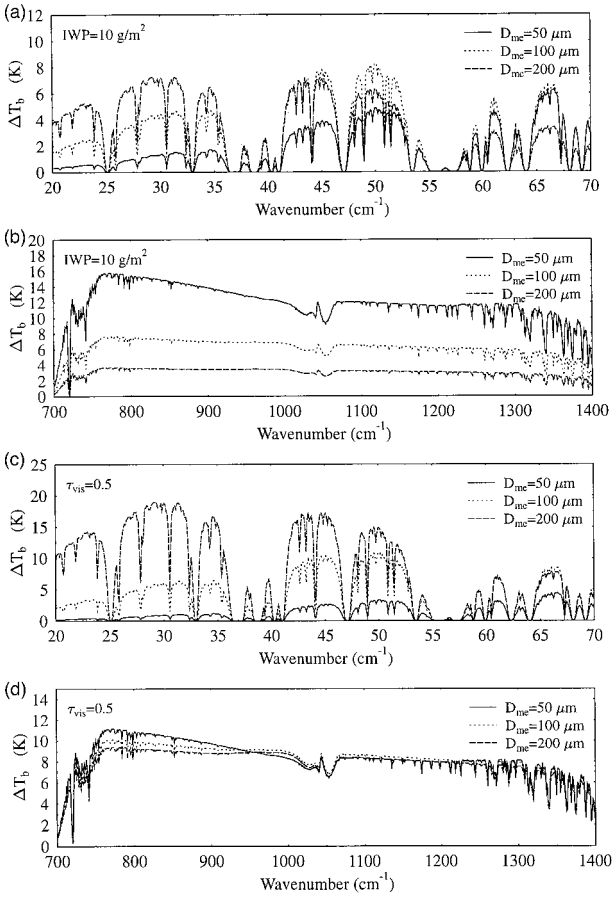

FIG. 3. The submillimeter and mid-IR nadir brightness temperature change modeled for cirrus clouds with different median ice sphere diameters, D_{me}. (a) and (b) Fixed ice water path of 10 g m^{-2}. (c) and (d) Fixed visible optical depth of 0.5. The submillimeter resolution is 0.1 cm^{-1}, while the mid-IR spectra resolution is 1.0 cm^{-1}. The cirrus cloud is from 9 to 10 km in a standard midlatitude winter atmosphere, and the observation altitude is 12 km.

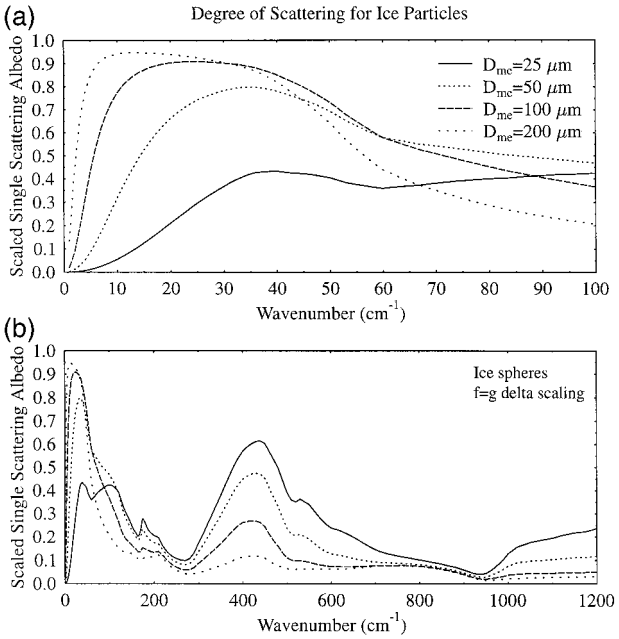

FIG. 4. (a) Dependence on the median equivalent volume sphere diameter (D_{me}). (b) The spectral response of the degree of scattering as measured by the delta-scaled single-scattering albedo for ice spheres.

at 52 cm^{-1} the ΔT_b of D_{me} = 200 μm and 50 μm are about the same.

The radiative processes behind the sensitivity to cirrus are quite different between the submillimeter and the infrared. The bulk absorption of ice is small below 40 cm^{-1}, and so submillimeter radiation interacts with cirrus ice particles primarily by scattering. The degree of scattering behavior is quantified by plotting the delta-scaled single-scattering albedo as a function of wavenumber for different particle sizes (Fig. 4). For median equivalent volume sphere diameters above 50 μm, submillimeter radiation interacts with cirrus clouds primarily by scattering. This region of high scattering extends to about 50 cm^{-1}. Note that smaller particles (e.g., D_{me} = 25 μm) never enter the scattering regime. The region around 400 cm^{-1} shows a strong dependence of single-scattering albedo on particle size, while the mid-infrared is mainly absorptive. The low absorption of cirrus ice particles in the submillimeter implies that the temperature of the cloud has only a minor effect on the upwelling radiance because emission has a small effect. The highly scattering behavior of ice particles in the submillimeter means that the radiance does not saturate at a visible optical depth of 4 as do mid-IR emission methods. Instead, the submillimeter brightness temperature decreases well below the cloud-top temperature for optically thicker clouds. Furthermore, the reduced sensitivity of the lower wavenumbers is an advantage because there will usually be a linear relationship between ΔT_b and IWP. This linearity implies that horizontal and vertical inhomogeneities are unimportant; that is, the ΔT_b signal is proportional to the integrated ice mass and the particle size measured is that of the whole cloud rather than the top.

The submillimeter sensitivity to a cirrus cloud is decreased as the cloud is moved lower in the atmosphere because water vapor absorption reduces the transmission to the cloud. The effect of cloud height on the ΔT_b becomes more significant with increasing wavenumber. The numerous strong water vapor lines in the spectrum, however, may allow for correction of the transmission above the cirrus cloud. The spectrometer measures the brightness temperature T_b, not the difference from clear-sky ΔT_b, and so implicitly the ''background'' clear-sky spectrum is required to derive the cirrus signal. The oxygen and water vapor absorption lines in the submillimeter may provide a means to infer the temperature and water vapor profiles that determine the background radiance.

TABLE 2. The setup and results for the linear inversion analysis. The 13 parameters of the base case and the perturbations are listed: IWP is ice water path, D_{me} is median particle diameter, α is gamma size distribution parameter, Z_{top} is cloud top height, ΔZ is cloud thickness, T is the layer temperature, RH is layer relative humidity. The ''random error'' is the standard error assuming random FTS spectral noise.

Parameter	Base case	Perturbation	Random error
IWP (g m^{-2})	10	+2	2.4
D_{me} (μm)	100	+20	5.3
α	1	+1	3.7
Z_{top} (km)	10	+0.25	0.4
ΔZ (km)	1.0	+0.25	0.8
T_{4-6} (K)	261	+1	19.0
T_{6-8} (K)	247	+1	4.6
T_{8-10} (K)	230	+1	1.1
T_{10-12} (K)	215	+1	0.1
RH_{4-6} (%)	57	×1.2	184
RH_{6-8} (%)	57	×1.2	87
RH_{8-10} (%)	69	×1.2	21
RH_{10-12} (%)	49	×1.2	2

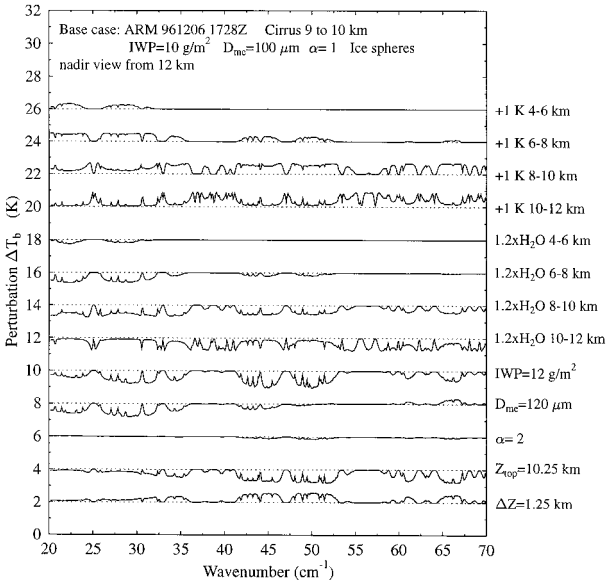

FIG. 5. The difference spectra from the base case for the 13 atmospheric perturbations. Each spectrum is shifted up 2 K from the previous one.

b. Linear inversion analysis

We seek to calculate the information content of the submillimeter spectra in order to determine the potential for retrieving cirrus parameters in spite of the uncertainties in background radiance and cloud-to-spectrometer transmission. This may be accomplished with a linear retrieval analysis. Spectra for 20–70 cm^{-1} at 0.1 cm^{-1} resolution are generated for a ''base'' case and for perturbations of various parameters around the base case. The 13 perturbations consist of variations in IWP, median particle size, size distribution width, cloud height, cloud thickness, and temperature and water vapor of four 2-km-thick layers (see Table 2). The base atmospheric profile (ARM 6 December 1996 1728 UTC) is quite warm and moist for winter, with the tropopause at 12 km, freezing level at 3 km, and relative humidity varying from 40% to 80% for the 4–12-km region.

In a linear analysis the spectra can be predicted from the perturbation parameters using a matrix:

$$T_i - T_i^{(0)} = \sum_j a_{ij}(x_j - x_j^{(0)}),$$

where T_i is the brightness temperature for the ith wavenumber, x_j is the atmospheric parameter vector, and $x_j^{(0)}$ are the base case parameters. The matrix elements are found from the differences between each perturbation and the base spectra according to

$$a_{ij} = \frac{T_i^{(j)} - T_i^{(0)}}{\delta x_j},$$

where δx_j is the amount the jth parameter is perturbed. The spectral differences for the 13 perturbations are shown in Fig. 5. The parameters clearly have different effects on the spectrum. The parameter uncertainties in the linear inversion can be derived from the random measurement noise. We assume the random noise σ_{T_i} is proportional to $1/\nu^2$ and is 1 K at 30 cm^{-1}. The random instrument noise is included in the analysis by defining

$$A_{ij} = \frac{a_{ij}}{\sigma_{T_i}} \quad \text{and} \quad b_i = \frac{T_i - T_i^{(0)}}{\sigma_{T_i}},$$

so that the linear system can be written as a matrix equation,

$$\mathbf{A}(\mathbf{x} - \mathbf{x}_0) = \mathbf{b}.$$

In this case $\mathbf{A}$ is a 500 row by 13 column matrix. The vector $\mathbf{b}$ is the deviation of the brightness temperature spectrum from the base case in terms of the signal-to-noise ratio. The least squares solution is

$$\mathbf{x} - \mathbf{x}_0 = (\mathbf{A}^T\mathbf{A})^{-1}\mathbf{A}^T\mathbf{b}.$$

The covariance matrix of the perturbation spectra is $\mathbf{A}^T\mathbf{A}$. Assuming independent random noise on the spectrum, which is appropriate for an FTS, the standard errors in the retrieved parameters are

$$\sigma_{x_j} = [(\mathbf{A}^T\mathbf{A})^{-1}]_{jj}^{1/2}.$$

The standard errors for the 13 parameters are listed in Table 2. The standard errors in cirrus parameters from the random noise are relatively small (2.4 g m^{-2} in IWP, 5 μm in D_{me}). This promising behavior is a result of the submillimeter spectra containing independent information about the parameters, and the averaging effect of 500 spectral points on the random noise. The perturbations in water vapor and temperature down to 4 km ensure that the effects of variability in the upwelling radiance below the cirrus is taken into account. The ability to retrieve the temperature and humidity of the lower layers is very poor because temperature and water

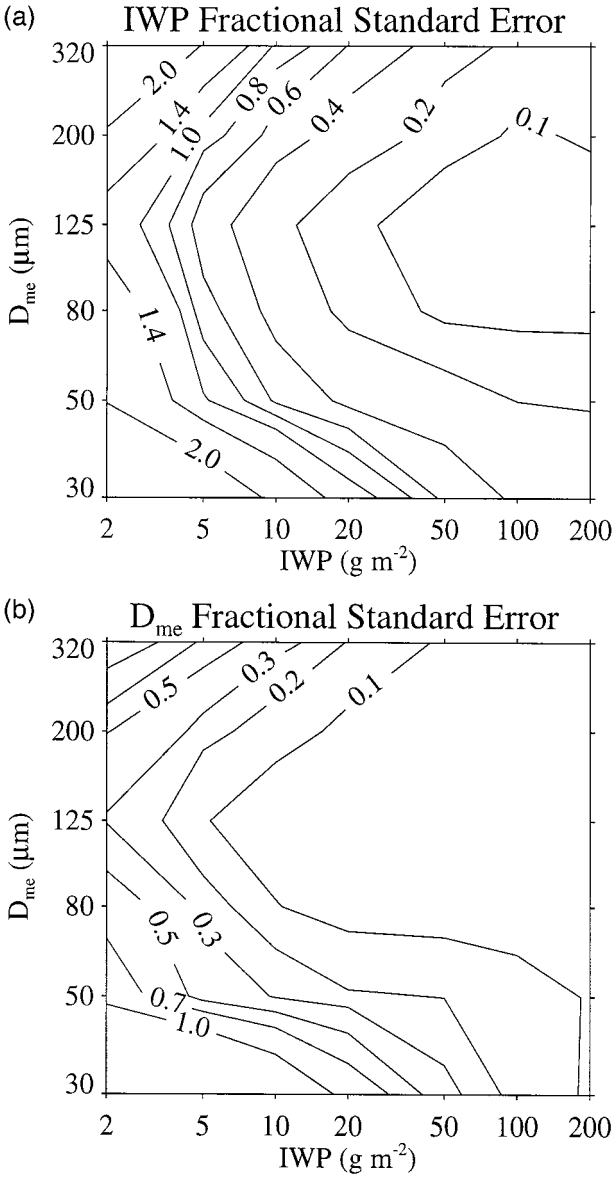

FIG. 6. The fractional error in (a) IWP and (b) median particle size (D_{me}) inferred from the linear inversion analysis. The base case is from Table 2, except IWP and D_{me} vary across the contour plot.

vapor have opposite spectral effects (-0.994 correlation for the 4–6-km layer). Temperature and water vapor profiling of the upper troposphere seems quite feasible. The perturbation spectra for cloud-top height and cloud thickness are highly correlated. This results in a large retrieval error for cloud thickness, though a cloud-height retrieval may be usable.

The results in the table are for just one base case, but it is useful to examine how the error depends on the cirrus parameters. Figure 6 show the fractional standard error in IWP and D_{me} as a function of base case IWP and D_{me}. The other parameters are as specified in Table 2. The fractional error in both IWP and D_{me} increases as the IWP decreases due to reduced signal to noise. There is also more retrieval error for the smaller particle sizes ($D_{me} < 80$ μm) and the larger particle sizes. The IWP error is about half for a cloud top of 11 km, but considerably larger for lower cloud heights. The high sensitivity of the linear retrieval error on cloud height is due to the high amount of upper tropospheric water vapor in this particular profile.

The linear inversion analysis is limited in that it does not take into account nonlinear retrieval errors, although it does include the effects of noise amplification by the inversion process. A nonlinear algorithm may not have as large rms errors where the linear inversion errors are high, but these will be the regions where the retrieval is difficult. The linear inversion analysis provides guidance on the level of accuracy that may be obtained for various parameters in designing an actual cirrus retrieval algorithm.

5. A simple retrieval algorithm and error analysis

A retrieval algorithm is described and tested in order to demonstrate the viability of the submillimeter spectrometer technique for cirrus remote sensing. Based on the results of the linear inversion analysis we choose to retrieve the cirrus IWP and median particle size (D_{me}).

a. The retrieval algorithm

The major difficulty in designing an algorithm to retrieve cirrus cloud properties from the FIRSC data is the large number of individual radiances in each spectrum. An iterative procedure that matches the spectra with line-by-line radiative transfer is computationally prohibitive. Thus, a method is needed to efficiently reduce the number of observables. We use a principle component [or empirical orthogonal function (EOF)] analysis to linearly project the spectra to a small number of ''pseudochannels.'' The 20 000 spectra database described in section 3b is used for the EOF analysis. As with the linear inversion analysis, the optimal procedure for dealing with the spectrally varying noise is to convert the spectra to signal-to-noise ratio by dividing the brightness temperature at each wavenumber by the standard deviation of the noise. After subtracting the mean spectrum from each database spectrum, the 500×500 spectrum covariance matrix is computed. The eigenvectors of the covariance matrix that explain the most variance are the ones used. The first six eigenvectors explain more than 99% of the variance in the spectra. A spectrum is converted to signal-to-noise ratio and projected onto the selected eigenvectors to make the pseudochannel values.

The relationship between cirrus parameters and the observed radiances (or pseudochannels) is nonlinear, and so multiple linear regression methods are not adequate. Nonlinear methods of fitting the forward-modeled data can, however, be used to derive cirrus prop-

erties as a function of the pseudochannels values. To perform this nonlinear fitting we chose the neural network program NNfit 2.0 (P. Cloutier, C. Tibirna, B. P. A. Grandjean, and J. Thibault, available on the World Wide Web at www.gch.ulaval.ca/~nnfit). The neural net model is an input layer of units, one hidden layer of neurons, and an output layer of neurons. The output H_j of the J hidden layer neurons is related to the I input unit values U_i by

$$H_j = f\left[\sum_{i=1}^{I+1} W_{ij}U_i\right] \qquad 1 \le j \le J, \tag{2}$$

where f is the sigmoid function $f(z) = (1 + e^{-z})^{-1}$. The hidden layer values are input to the output layer neurons, producing the neural net output S_k by

$$S_k = f\left[\sum_{j=1}^{J+1} W_{jk}H_j\right] \qquad k = 1, \tag{3}$$

and here we have only one output value. The last input unit U_{I+1} and last hidden unit H_{J+1} are fixed at unity. The I pseudochannel values are normalized (0, 1) to make the input units U_i. The weights W_{ij} and W_{jk} connect neurons in one layer with those in the next layer. The weights thus contain the nonlinear fitting information, and NNfit adjusts them during the training procedure to minimize the rms error between the neural net output S and the normalized input cirrus parameter.

The neural net is trained with brightness temperature spectra to which Gaussian noise, $[\sigma = 1 \text{ K } (30 \text{ cm}^{-1}/\nu)]^2$, has been added. The learning database for the neural net is 10 noise realizations for each of the 20 000 spectra. A separate neural net training is done for each of the two retrieved cirrus parameters, ln(IWP) and ln(D_{me}). The number of pseudochannels and hidden units is found by increasing them until little further effect on the overall rms fitting error is noticed. The algorithm uses 15 pseudochannels and 20 hidden neurons for a total of 341 weights. The resulting algorithm consists of the database mean spectrum and the eigenvectors for producing the 15 pseudochannels and the neural net weights for each retrieved cirrus parameter.

b. Assessment of algorithm accuracy

The accuracy of the neural network cirrus retrieval algorithm is determined theoretically with a Monte Carlo procedure. Synthetic brightness temperature spectra are computed with radiative transfer modeling, noise is added, and cirrus properties are retrieved and compared. To determine the accuracy as a function of cirrus properties, a $7 \times 5 \times 4$ grid of IWP, median particle size (D_{me}), and cloud-top height (Z_{top}) are chosen. For each IWP, D_{me}, and Z_{top} point, 50 spectra are simulated, using 50 ARM radiosonde profiles from December 1995, random cloud thicknesses, and internal inhomogeneity parameters. The spectra database made for the testing is independent of the one used in training the neural net. Ten realizations of noisy spectra are made by adding independent Gaussian noise with the appropriate standard deviation. The retrieval algorithm is then run using the 500 spectra for each of the 140 IWP, D_{me}, Z_{top} gridpoints.

The error is assessed by comparing the retrieved IWP and D_{me} to the known values. The rms and mean logarithmic differences are exponentiated to compute error factors, for example,

$$\text{rms error factor} = \exp\left\{\left[\frac{1}{N}\sum_{i=1}^{N}(\ln\text{IWP}_i^{\text{ret}} - \ln\text{IWP}_i^{\text{true}})^2\right]^{1/2}\right\}. \tag{4}$$

For small rms error factors, 1 may be subtracted to obtain the one standard deviation fractional error (e.g., a factor of 1.3 implies about 30% error). Figure 7 shows the IWP error factor for cloud tops of 10 km. The IWP error factor is below a quite usable value of 1.5 for IWP > 5 g m^{-2} and $D_{\text{me}} > 60$ μm, and the error is only about 30% for IWP > 50 g m^{-2} The IWP error increases for lower IWP due to reduced signal-to-noise ratio. As expected from the linear analysis, the errors increase for the smallest and largest median particle sizes. The IWP bias is positive for low IWP but negative for the smaller median particle sizes.

We expect the errors to increase substantially for lower cirrus clouds as the transmission is reduced by water vapor absorption. Figure 8 shows that the error is relatively constant for clouds with tops above 10 km but increases for lower clouds. For cloud tops of 8 km the IWP errors are rather large, showing that information from additional sensors is required for adequate IWP retrieval.

Figure 9 shows the rms and bias errors for median particle size D_{me}. The rms error is below 20% for a large portion of the domain. The error increases for sizes above and below 70 μm, especially for lower IWP. It is clear from the bias plot that the neural net retrieval is pulling the D_{me} retrieval toward 70 μm when the signal-to-noise ratio is poor.

We made a number of assumptions, such as spherical particles and winter atmospheres, in developing the retrieval algorithm and subsequent testing. The effects of these assumptions is now briefly explored. Cirrus retrievals using synthetic spectra made with the standard assumptions are compared to retrievals using spectra calculated with other assumptions. The ''standard'' case has a midlatitude winter atmosphere with a cirrus cloud of ice spheres from 9 to 10 km (the relative humidity of these levels is set to 60%). Cirrus retrievals are performed on 100 realizations of noisy spectra. The rms retrieval errors for three different ice clouds (values of IWP and D_{me}) are shown in Table 3. The standard case typically has 20% errors in IWP retrieval. Assuming the cirrus cloud is made of randomly oriented cylinders instead of ice spheres does not change the IWP errors

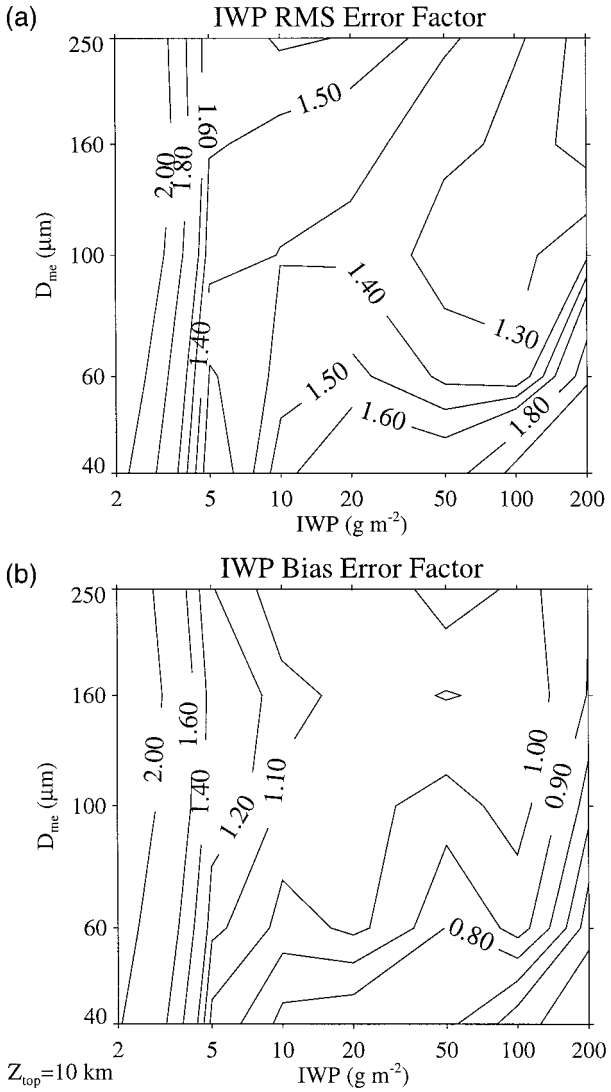

FIG. 7. The (a) rms and (b) bias error factors in retrieved IWP as a function of IWP and median particle size (D_{me}) for cloud-top heights of 10 km. An error factor of 1 implies no error.

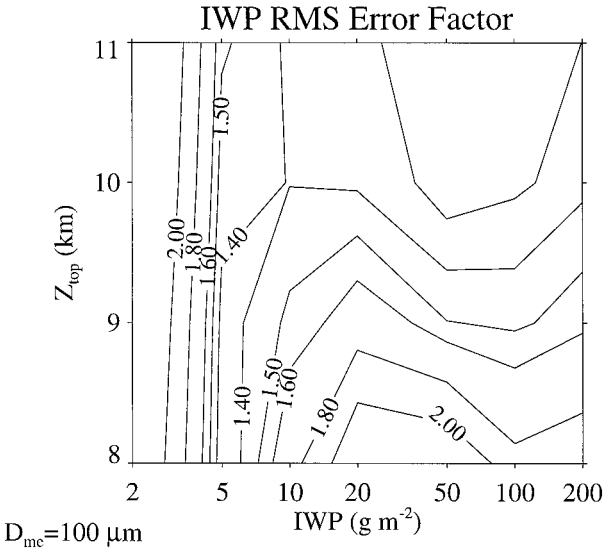

FIG. 8. The rms error factor in retrieved IWP as a function of IWP and cloud top height (Z_{top}) for cirrus with median particle size D_{me} = 100 μm.

significantly; it mainly changes the error pattern. The effect of a nonwinter atmospheric profile is considered by using the ARM radiosonde profile from 1730 UTC on 16 April 1996. This profile has a 12-km tropopause, a surface temperature of 25°C, and a 59% humidity at 9 km. The retrieval errors for the April atmosphere are not significantly different. The effect of a supercooled water cloud below the ice-cloud layer is judged by simulating a liquid cloud from 6 to 7 km. This typical altostratus cloud has a cloud-top temperature of −36°C, an LWP of 30 g m^{-2}, effective radius of 5 μm, and visible optical depth of 9. The retrieval errors are not significantly different from the standard case. The effect of the hybrid radiative transfer model accuracy is gauged by performing retrievals on spectra computed with the multistream doubling–adding code. Again the retrieval errors are equivalent to the standard case. These tests indicate that the assumptions made in developing this submillimeter cirrus retrieval algorithm are not profoundly limiting.

6. Summary and conclusions

A new technique for remote sensing cirrus cloud properties from spacecraft or high-altitude aircraft is explored with modeling. This work is motivated by deployment of a Fourier transform spectrometer instrument, the FIRSC, with spectral coverage from 10 to 135 cm^{-1}. The modeling focuses on the submillimeter region from 20 to 70 cm^{-1}, where the most promising cirrus signatures are found. Due to the wide range of wavelengths comparable to the cirrus particle sizes, this technique has much greater sensitivity to particle size for median mass diameters D_{me} above 50 μm than infrared methods. The submillimeter brightness temperature change due to cirrus is more related to the IWP than is the infrared and visible signals, which are related to visible optical depth. Also in contrast with the infrared, radiation below 50 cm^{-1} interacts with ice particles (for $D_{me} > 50$ cm^{-1}) primarily by scattering rather than absorption and emission. This independent physical basis for remote sensing is advantageous because cloud temperature is not important and signal saturation does not occur for moderate optical depths. A linear inversion analysis is done to illustrate how the cirrus properties, water vapor profile, and temperature profile affect the submillimeter radiance spectrum differently. Based on the linear inversion retrieval errors, it appears that a submillimeter spectrometer can accurately measure cirrus IWP, particle size, and upper-tropospheric temperature and water vapor.

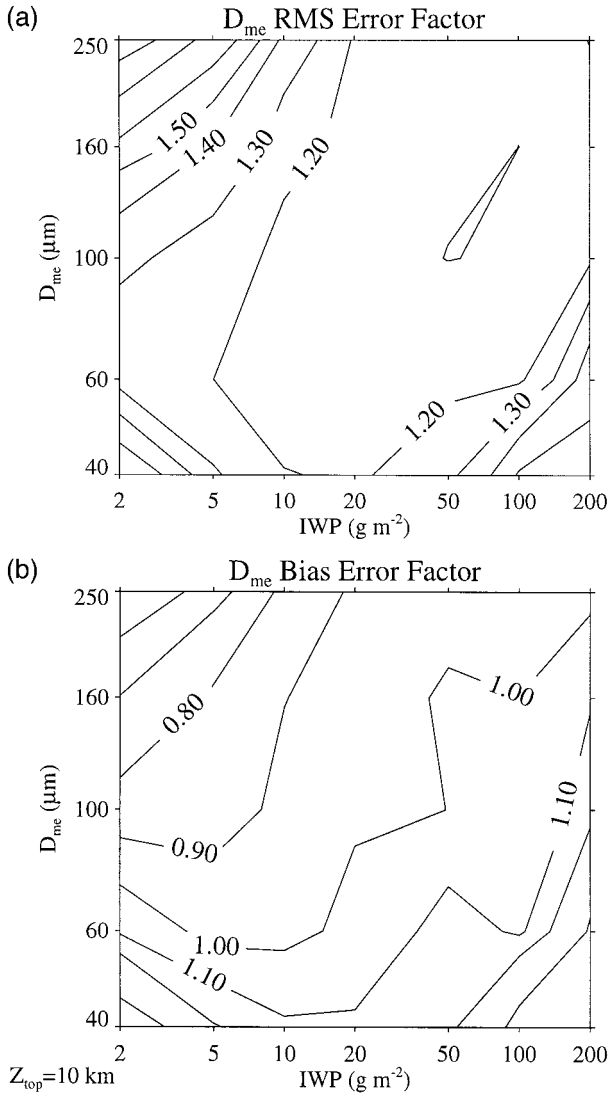

FIG. 9. The rms and bias error factors in (a) retrieved median particle size (D_{me}) as a function of IWP and (b) D_{me} for cloud-top heights of 10 km.

TABLE 3. Comparison of cirrus IWP and D_{me} retrieval error for spectra simulated using other assumptions.

Case	IWP (g m^{-2}) 10	D_{me} (μm) 100	IWP (g m^{-2}) 30	D_{me} (μm) 100	IWP (g m^{-2}) 30	D_{me} (μm) 200
Standard	1.2	8.8	7.2	7.8	4.4	8.1
Ice cylinders	2.1	7.3	2.4	4.6	8.5	8.2
April atmosphere	1.2	9.7	5.5	4.2	5.3	9.2
Lower water cloud	1.3	11.0	5.7	8.2	4.8	5.4
Multistream code	2.0	7.7	3.8	7.7	8.3	8.2

A nonlinear statistical retrieval algorithm is developed and tested to illustrate the potential accuracy of the submillimeter spectrometer technique for remote sensing cirrus properties. A database of 20 000 radiance spectra is constructed using a wide variety of cirrus cloud properties and atmospheric radiosonde profiles. The cirrus IWP, median sphere diameter, size distribution width, cloud height, thickness, and vertical inhomogeneity are varied randomly. The spectra database is developed for nadir viewing from a 12-km flight altitude in winter at a midcontinental U.S. location. An empirical orthogonal function analysis is used to project the 500-point spectra to 15 principal components or pseudochannels. The pseudochannels with realistic noise added are used to train a neural network to retrieve cirrus IWP and D_{me}. The retrieval accuracy is determined as a function of ice water path, particle size, and cloud height with a Monte Carlo retrieval process using an independent spectra database. For cloud tops of 10 km, the rms IWP error factor ranges from 1.3 to 1.5 for IWP $>$ 5 g m^{-2} and $D_{me} > 60$ μm and $D_{me} < 200$ μm. The rms errors in D_{me} are mostly less than 20% for this range of parameter space. These error estimates are comparable to those in Evans et al. (1998), although that analysis included the effects of ice particle shape but not atmospheric profile variability.

The retrieval algorithm was developed with ice sphere scattering, and the issue of particle shape was only briefly explored. This may be adequate for nadir viewing, but it certainly is not for an off-nadir viewing polarization sensing instrument because significant polarization signatures are expected for oriented particles. The performance of the submillimeter cirrus sensing technique with mixed-phase clouds needs to be investigated further. However, due to water vapor absorption, the sensitivity to lower ice clouds is reduced, thereby lessening the importance of mixed-phase clouds.

The statistical retrieval algorithm is limited and mainly suitable as a preliminary algorithm. The neural net retrieval must be trained for each flight situation (viewing angle, flight altitude, atmospheric climatology). It is difficult to determine whether enough training cases have been presented to the network. Although the neural net algorithm is robust to noise, it is biased toward the statistical mean and is totally unable to extrapolate beyond the range of its training database. We plan to implement a retrieval algorithm based on a fast radiative transfer method to make the algorithm more flexible. We expect this type of retrieval algorithm to be more accurate than the one presented here, and the ability to use auxiliary data such as soundings or other radiometric data should improve the accuracy further.

Test flights of the FIRSC instrument occurred in April and May 1998. The analysis of spectra from these flights will be reported later. We hope to upgrade the instrument capability to measure off-nadir radiances for two polarizations. Oblique viewing angles will increase the sensitivity to cirrus ice mass and the polarization measurement will provide information about ice particle shape. Looking to the future, the far infrared FTS technology exists for a spacecraft instrument that would allow important cirrus properties such as ice water path

and particle size to be measured accurately on a global basis.

Acknowledgments. Sounding data were obtained from the Atmospheric Radiation Measurement Program sponsored by the U.S. Department of Energy. Financial support to KFE and AHE for this research was provided by NASA FIRE-III Grant NAG1-1702. Support for the FIRSC instrument development has been provided by the LaRC Space Technology and Thrust Office, Atmospheric Science Division, and a LaRC Director's Discretionary Fund Grant.

REFERENCES

Carli, B., F. Mencaraglia, and A. Bonetti, 1984: Submillimeter high resolution FT spectrometer for atmospheric studies. *Appl. Opt.,* **23,** 2594–2603.

Clough, S. A., 1994: Radiative transfer model development in support of the atmospheric radiation measurement program. *Proc. Third ARM Science Team Meeting,* Norman, OK, Department of Energy, 11–17.

Deeter, M. N., and K. F. Evans, 1998: A hybrid Eddington-single scattering radiative transfer model for computing radiances from thermally emitting atmospheres. *J. Quant. Spectrosc. Radiat. Transfer,* **60,** 635–648.

Dickinson, P., B. Carli, P. Ade, I. Nolt, J. Leotin, and M. Carlotti, 1995: SAFIRE—An airborne far infra-red limb sounder. *S.P.I.E. Global Process Monitoring and Remote Sensing of the Ocean and Sea Ice,* Vol. 2586, D. W. Deering and P. Gudmandsen, Eds., SPIE, 214–224.

Evans, K. F., and G. L. Stephens, 1991: A new polarized atmospheric radiative transfer model. *J. Quant. Spectrosc. Radiat. Transfer,* **46,** 412–423.

——, and ——, 1995: Microwave radiative transfer through clouds composed of realistically shaped ice crystals. Part II: Remote sensing of ice clouds. *J. Atmos. Sci.,* **52,** 2058–2072.

——, S. J. Walter, A. J. Heymsfield, and M. N. Deeter, 1998: Modeling of submillimeter passive remote sensing of cirrus clouds. *J. Appl. Meteor.,* **37,** 184–205.

Fowler, L. D., D. Randall, and S. Rutledge, 1996: Liquid and ice cloud microphysics in the CSU general circulation model. Part I: Model description and simulated microphysical processes. *J. Climate,* **9,** 489–529.

Gasiewski, A. J., 1992: Numerical sensitivity analysis of passive EHF and SMMW channels to tropospheric water vapor, clouds, and precipitation. *IEEE Trans. Geosci. Remote Sens.,* **30,** 859–870.

Giraud, V., C. Buriez, Y. Fouquart, and F. Parol, 1997: Large-scale analysis of cirrus clouds from AVHRR data: Assessment of both a microphysical index and the cloud-top temperature. *J. Appl. Meteor.,* **36,** 664–675.

Gordley, L. L., B. T. Marshall, and D. A. Chu, 1994: LINEPAK: Algorithms for modeling spectral transmittance and radiance. *J. Quant. Spectrosc. Radiat. Transfer,* **52,** 563–580.

Heymsfield, A. J., and G. M. McFarquhar, 1996: High albedos of cirrus in the tropical Pacific warm pool: Microphysical interpretations from CEPEX and from Kwajalein, Marshall Islands. *J. Atmos. Sci.,* **53,** 2424–2451.

Inoue, T., 1985: On the temperature and effective emissivity determination of semitransparent cirrus clouds by bispectral measurements in the 10 μm window region. *J. Meteor. Soc. Japan,* **63,** 88–98.

Liou, K.-N., 1986: Influence of cirrus clouds on weather and climate processes. *Mon. Wea. Rev.,* **114,** 1167–1199.

Martin, D. H., and E. Puplett, 1969: Polarized interferometric spectrometry for the millimeter and submillimeter spectrum. *Infrared Phys.,* **10,** 105–109.

Minnis, P., K.-N. Liou, and Y. Takano, 1993: Inference of cloud cirrus properties using satellite-observed visible and infrared radiances. Part I: Parameterization of radiance fields. *J. Atmos. Sci.,* **50,** 1279–1304.

Mishchenko, M. I., L. D. Travis, and D. W. Mackowski, 1996: T-matrix computations of light scattering by nonspherical particles: A review. *J. Quant. Spectrosc. Radiat. Transfer,* **55,** 535–575.

Nolt, I. G., and L. P. Stearns, 1980: Infrared water vapor measurements from the Kuiper airborne observatory. *Atmospheric Water Vapor,* A. Deepak, T. D. Wilkinson, and L. Ruhnke, Eds., Academic Press, 343–354.

——, and Coauthors, 1997: Stratospheric HBr concentration profile obtained from far infrared emission spectroscopy. *Geophys. Res. Lett.,* **24,** 281–284.

Ou, S. C., K. N. Liou, W. M. Gooch, and Y. Takano, 1993: Remote sensing of cirrus cloud parameters using advanced very-high-resolution radiometer 3.7- and 10.9-μ channels. *Appl. Opt.,* **32,** 2171–2180.

Stephens, G. L., and P. J. Webster, 1981: Clouds and climate: Sensitivity of simple systems. *J. Atmos. Sci.,* **38,** 235–247.

——, S. C. Tsay, J. P. W. Stackhouse, and P. Flatau, 1990: The relevance of the microphysical and radiative properties of cirrus clouds to climate and climatic feedback. *J. Atmos. Sci.,* **47,** 1742–1753.

Warren, S. G., 1984: Optical constants of ice from the ultraviolet to the microwave. *Appl. Opt.,* **23,** 1206–1225.

Wielicki, B.-A., and Coauthors, 1990: The 27–28 October 1986 FIRE IFO cirrus case study: Comparison of radiative transfer theory with observations by satellite and aircraft. *Mon. Wea. Rev.,* **118,** 2356–2376.

——, R. D. Cess, M. D. King, D. A. Randall, and E. F. Harrison, 1995: Mission to Planet Earth: Role of clouds and radiation in climate. *Bull. Amer. Meteor. Soc.,* **76,** 2125–2153.

Wylie, D. P., W. P. Menzel, H. M. Woolf, and K. I. Strabala, 1994: Four years of global cirrus cloud statistics using HIRS. *J. Climate,* **7,** 1972–1986.